High intensity vacuum ultraviolet and extreme ultraviolet production by noncollinear mixing in laser vaporized media

Michael A. Todt, Daniel R. Albert, and H. Floyd Davis

Citation: Review of Scientific Instruments **87**, 063106 (2016); doi: 10.1063/1.4952749
View online: http://dx.doi.org/10.1063/1.4952749
View Table of Contents: http://aip.scitation.org/toc/rsi/87/6
Published by the American Institute of Physics

Articles you may be interested in

High-intensity coherent vacuum ultraviolet source using unfocussed commercial dye lasers
Review of Scientific Instruments **84**, 063104 (2013); 10.1063/1.4806801

Vacuum-ultraviolet frequency-modulation spectroscopy
The Journal of Chemical Physics **146**, 014201 (2017); 10.1063/1.4973011

Communication: On the first ionization threshold of the C_2H radical
The Journal of Chemical Physics **146**, 011101 (2017); 10.1063/1.4973383

Observation of enhanced rate coefficients in the $H_2^+ + H_2 \rightarrow H_3^+ + H$ reaction at low collision energies
The Journal of Chemical Physics **145**, 244316 (2016); 10.1063/1.4972130

Electronic spectrum and photodissociation chemistry of the linear methyl propargyl cation $H_2C_4H_3^+$
The Journal of Chemical Physics **146**, 044307 (2017); 10.1063/1.4974338

Advantage of spatial map ion imaging in the study of large molecule photodissociation
The Journal of Chemical Physics **147**, 013904 (2017); 10.1063/1.4975671

REVIEW OF SCIENTIFIC INSTRUMENTS **87**, 063106 (2016)

High intensity vacuum ultraviolet and extreme ultraviolet production by noncollinear mixing in laser vaporized media

Michael A. Todt, Daniel R. Albert, and H. Floyd Davis[a)]
Baker Laboratory, Department of Chemistry and Chemical Biology, Cornell University, Ithaca, New York 14853-1301, USA

(Received 30 October 2015; accepted 16 May 2016; published online 13 June 2016)

A method is described for generating intense pulsed vacuum ultraviolet (VUV) and extreme ultraviolet (XUV) laser radiation by resonance enhanced four-wave mixing of commercial pulsed nanosecond lasers in laser vaporized mercury under windowless conditions. By employing noncollinear mixing of the input beams, the need of dispersive elements such as gratings for separating the VUV/XUV from the residual UV and visible beams is eliminated. A number of schemes are described, facilitating access to the 9.9–14.6 eV range. A simple and convenient scheme for generating wavelengths of 125 nm, 112 nm, and 104 nm (10 eV, 11 eV, and 12 eV) using two dye lasers without the need for dye changes is described. *Published by AIP Publishing.* [http://dx.doi.org/10.1063/1.4952749]

I. INTRODUCTION

Four-wave sum frequency mixing of commercial tunable nanosecond pulsed lasers in gases is a well-established method for producing coherent vacuum ultraviolet (VUV, $\lambda < 180$ nm) and extreme ultraviolet (XUV, $\lambda < 110$ nm) radiation.[1–3] A thorough summary of current XUV and VUV generation methods and uses, written by Eikema and Ubachs, can be found in the *Handbook of High Resolution Spectroscopy*.[4] These wavelengths span photon energies where gaseous molecules undergo photodissociation and/or photoionization. Many schemes employing inert gases (particularly Kr and Xe) have been reported with the greatest efficiencies obtained by exploiting the large resonance enhancements in $\chi^{(3)}$ in the vicinities of one- and two-photon resonances.[5] In certain wavelength regions, conversion efficiencies can be further improved by optimal phase matching using gas mixtures.[5–7] By employing resonance enhancement and phasematching simultaneously, conversion efficiencies approaching 0.1% can be achieved under favorable conditions in Kr or Xe.[5,7]

The extremely large nonlinear susceptibilities of metallic gases such as mercury (Hg) lead to conversion efficiencies into the VUV/XUV that can be orders of magnitude greater than that for inert gases.[1,8–10] For example, by tuning a single frequency-doubled dye laser to the 6 $^1S_0$-7 $^1S_0$ two-photon resonance in Hg at 312.85 nm, and mixing in the residual 625.70 nm fundamental, $\sim 10^{13}$ photons/pulse near 10 eV can be produced in a focused configuration using heated cell.[9,10] This corresponds to conversion efficiencies from the UV greater than 1%.[9,10] We recently described schemes for mixing of two or three collimated (unfocused) beams from commercial dye lasers in 1 m long Hg heat pipes for production of ~0.1 mJ pulses (6×10^{13} photons/pulse) near 125 nm and 130 nm.[11] Because the laser beams are unfocused, by scaling the input laser beams to higher energies, VUV output pulse energies in the millijoule range are achievable.[12,13] In this wavelength range, MgF_2 and LiF optics can be employed for focusing or dispersing the VUV from the much more intense UV and visible beams with modest power losses, e.g., by transmission through a lens held off of the optical axis.[11,13,14]

The optical transmission of window materials decreases sharply at shorter wavelengths, falling to zero for LiF at $\lambda < 104$ nm.[15] For MgF_2, the only other material capable of transmitting light at $\lambda < 140$ nm, the transmission cutoff occurs at 116 nm.[15] Consequently, a number of windowless schemes have been developed for operation in the XUV.[16–19] One approach employs a capillary array to transmit XUV light from the high pressure region (where 4-wave mixing is carried out) to a low-pressure region such as the ionization source of a mass spectrometer.[16,19,20] For mixing in inert gases, a simple approach involves nonlinear conversion in pulsed gas jets.[21–25] Due to the very small gas load, the XUV can be propagated through a single differentially pumped aperture, thereby avoiding the need for window material or capillary arrays.

Many scientific applications require separation of the XUV from the much more intense residual UV and visible laser beams, usually requiring dispersion by a grating.[24,25] This approach is expensive, particularly because gratings are susceptible to optical damage by high-power laser beams. From a practical perspective, the efficiencies of gratings are typically only ~10%, severely limiting the usable XUV photon flux.

Clearly, four-wave mixing of commercial nanosecond lasers facilitates access to the VUV region with efficiencies sufficient for many scientific applications. Unfortunately, due to the need for windowless operation and the low efficiency of dispersive elements such as gratings, efficient access to the XUV region by nonlinear conversion of tabletop laser systems has remained quite challenging from an experimental perspective. In the present work, we sought an experimental approach that would increase conversion efficiencies, while simultaneously simplifying the experimental setup by eliminating the need for

a)Author to whom correspondence should be addressed. Electronic mail: hfd1@cornell.edu

capillary arrays, extensive differential pumping, and optical elements such as gratings.

If the two input laser beams are crossed at a small angle, four-wave mixing produces an output beam that propagates in a direction different from the residual input beams. This eliminates the need for dispersive elements such as gratings for wavelength separation.[4,26,27] To date, this approach has been carried out using inert gases (e.g., Xe) in static cells[26] or in pulsed jets[27] as the nonlinear medium. Peet and Tsubin compared the efficiencies for resonance-enhanced third harmonic generation in Xe using both collinear (single beam) and noncollinear (two crossed sub-beams) and found that both modes provide nearly the same conversion efficiencies but with different tuning curves.[26] It should be noted that noncollinear schemes have also been demonstrated theoretically and experimentally with femtosecond laser systems by nonresonant four-wave mixing in a transparent solid, e.g. LiF, CaF_2 or fused silica.[28–31] In these cases, the intersection angle of the input beams were chosen to optimize phase-matching conditions for four-wave mixing. In our experiments, the input wavelength is scanned to optimize phase-matching for a given crossing angle.

The use of a continuous Hg gas jet for VUV generation has been reported.[32] However, this approach is complex and could present a safety hazard due to the need for vaporizing and recycling large volumes of liquid Hg. Chénais and coworkers generated VUV in a Hg plume produced by laser vaporization from liquid Hg in a room temperature cell.[33] The use of laser vaporization of Hg is extremely attractive because very small Hg samples can be employed and no active pumping is needed to recirculate Hg. Furthermore, because the vapor pressure of Hg is 2×10^{-3} Torr at room temperature,[34] a single stage of differential pumping makes the windowless operation straightforward.

In the work reported by Chénais, only a single dye laser was available for generating the input beams, i.e., 625.70 nm and 312.85 nm corresponding to the fundamental and second harmonic of a DCM dye laser.[33] Therefore, the generated output beam (near 125 nm) was not tunable, and no attempt was made to separate the VUV from the residual input beams. They reported pulse energies up to 5 μJ (3×10^{12} photons/pulse), which were comparable to the values reported using heated cells.[33] We note that near 125 nm, the well-established heated cell method[9] with LiF or MgF_2 optics is simple and reliable. Therefore, the added complexity of a laser vaporization source (requiring an independently triggered Nd:YAG or excimer laser for vaporization) is probably not justified. However, for production of radiation at shorter wavelengths, especially where transmission through LiF or MgF_2 windows becomes inefficient or zero, the benefits of laser vaporization justify the added complexity.

Several articles have appeared reporting production of high VUV intensities (10^{13} photons/pulse) by four-wave mixing in *room temperature Hg in the absence of laser vaporization.*[35,36] While we were able to produce VUV using room temperature ambient Hg, the intensities were at least two orders of magnitude smaller than using heated Hg cells or the laser vaporization method described here.

Difference frequency mixing ($2\omega_1 - \omega_3 = \omega_{VUV}$) in inert gases facilitates production of broadly tunable VUV.[7] Sum frequency mixing schemes ($2\omega_1 + \omega_3 = \omega_{VUV}$) producing broadly tunable XUV have also been described.[23–25] However, for many applications, broad tunability is not necessary and instead the highest conversion efficiencies into the VUV or XUV are desirable at a single wavelength or over a limited wavelength range. For the production of VUV at photon energies below the Hg ionization limit (10.43 eV), the efficiencies for VUV production vary strongly with wavelength.[9,10] However, at higher energies, the XUV is continuously tunable.[19,20]

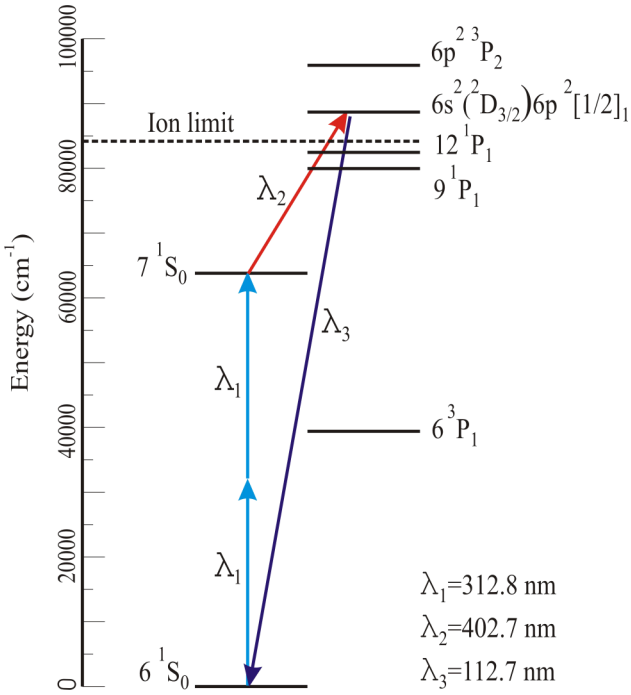

FIG. 1. Partial energy level diagram for Hg. Production of 112.7 nm light (11.0 eV) is illustrated.

We have employed noncollinear mixing of input laser beams in laser vaporized Hg to produce VUV and XUV wavelengths ranging from $\lambda = 125$ nm (9.9 eV) to $\lambda = 96.9$ nm (12.8 eV) utilizing the 6^1S_0-$7\ ^1S_0$ two photon resonance in Hg (Fig. 1). Comparisons are made between this method and the use of a standard heated cell configuration,[9] both in collinear and noncollinear geometries. Absolute VUV intensity measurements at 125 nm, 121 nm, 112 nm, 104 nm, and 96.9 nm are provided. Tuning curves through the $9\ ^1P_1$ and $12\ ^1P_1$ resonances in Hg are also provided for both collinear and noncollinear geometries. In addition, a number of wavelengths utilizing higher energy two photon resonances have also been explored, leading to higher energy photons (up to 14.6 eV) at lower intensities.

II. EXPERIMENTAL

The 312.85 nm light tuned to the $6\ ^1S_0$-$7\ ^1S_0$ two-photon transition in Hg was generated by frequency-doubling the output of a Nd:YAG pumped (Continuum Powerlite 8010, 532 nm, 8 ns/pulse, 10 Hz) tunable dye laser (either Lambda-Physik Scanmate 2 or FL3002) using DCM dye tuned to 625.7 nm. Visible and UV light were produced using a second tunable dye laser (Scanmate 2), pumped by either the

TABLE I. Summary of wavelengths used for VUV generation, pulse energy, VUV photon energy, dye used, and maximum number of photons produced per pulse.

λ_1 (nm)	Pulse energy (mJ)	λ_2 (nm)	λ_3 (nm)	Pulse energy (mJ)	λ_{VUV} (nm)	Photon energy (eV)	λ_3 laser dye	VUV photons per pulse
313	5.5	313	625	7.0	125	9.9	DCM	5×10^{12}
313	2.5	313	540	4.0	121	10.2	C540A[a]	2×10^{11}
313	3.0	313	403	5.5	112	11.0	Ex 404[b]	2×10^{11}
254	0.8	408	408	4.5	112	11.0	Ex 404[b]	5×10^{11}
313	2.5	313	312	2.5	104	11.9	DCM[c]	9×10^{10}
254	0.8	254	408	4.5	97	12.8	Ex 404[b]	2×10^{8}
269	1.0	269	269	1.0	90	13.8	C540A[a,c]	3×10^{7}
255	0.7	255	255	0.7	85	14.6	LDS 765[d]	6×10^{6}

[a]Coumarin 540A laser dye.
[b]Exalite 404 laser dye.
[c]Frequency doubled.
[d]Frequency tripled.

532 nm or 355 nm output from the same Nd:YAG laser. In the cases where $\lambda_3 < 400$ nm, the output of the second dye laser was frequency-doubled. Sum frequency mixing involved $\omega_{VUV} = 2\omega_1 + \omega_2$, with ω_{VUV} tunable by tuning ω_2. Table I summarizes pertinent information concerning the three input wavelengths (λ_1, λ_2, and λ_3) and the resulting λ_{VUV}.

The experimental setup is illustrated in Fig. 2. The two input laser beams (~2 mm diameter) were initially focused through the center of a 34 cm focal length achromatic lens (Optics for Research) and aligned through the Hg cell and interaction regions collinearly to produce maximum VUV intensities. The final mirrors for each input beam were mounted on separate translation stages. This made it possible to independently translate each beam away from the center of the lens, with one beam at the 3 o'clock and the other at the 9 o'clock positions on the lens. When in a non-collinear geometry, the VUV beam propagated at an angle between the two initial beams, determined by the input photon energies and crossing angle. In this case of $\lambda_1 = \lambda_2$, if the propagation of λ_1 laser is defined as $\theta = 0$, then $\theta_{VUV} = \theta_{crossing}[\omega_3/(2\omega_1 + \omega_3)]$.

Figure 3 shows a more detailed view of the ablation cell. The ablation cell was built using a 2.75 in. six-way conflat cross (MDC) with input and output arms each extended by 5 in. using stock 2.75 in. conflat nipples (MDC). The Hg reservoir is a 1 in. diameter stainless steel rod with a 3/4 in. diameter, 1/8 in. deep counterbore to contain the Hg. Water channels (0.25 in. dia.) were drilled through the length of the rod to allow cold water from a thermostatically controlled refrigerated bath (Neslab RTE-111) to be circulated, thereby cooling the mercury sample to ~7 °C. The vapor pressure of Hg at this temperature is ~4.1×10^{-4} Torr.[34] The 6-way cross was evacuated continuously by a small rotary vacuum pump connected via a needle valve. Even after many months of operation, the amount of Hg removed by the vacuum pump was negligible. The 1 in. diameter rod was sealed to the bottom of the 6-way cross using a Cajon fitting with o-ring seal, making it possible to translate the entire rod up and down to precisely locate the surface of the mercury pool relative to the laser axis. The laser input window was heated to ~30 °C (by wrapping the arm with heating tape) to prevent Hg buildup. The ablation source and detection chamber were separated by a double-sided 2 3/4 in. Conflat flange with a 1 mm diameter centrally located hole. The entire Hg cell assembly was sealed to the vacuum chamber via a 2.75 in. gate valve (MDC). The valve was kept closed except during experiments.

The degree of spatial separation of λ_{VUV} from λ_3 and λ_1 is directly related to the angle between the input beams introduced by walking the beams away from the central axis of the focusing lens. For a given crossing angle, as λ_3 decreases, the separation between the λ_1 and λ_{VUV} beams increases. For example, using 312.85 nm and 625 nm input beams, in order to separate the centers of the VUV and 312.85 nm beam

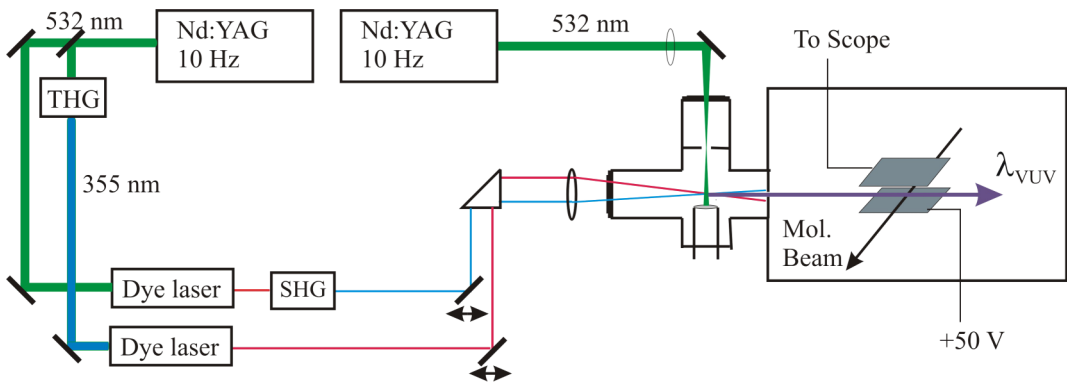

FIG. 2. Laser table layout. Output of each of the two dye lasers is temporally and spatially overlapped, with translation stages for each beam before being focused into the Hg cell. The detection method shown is the 2-plate detector.

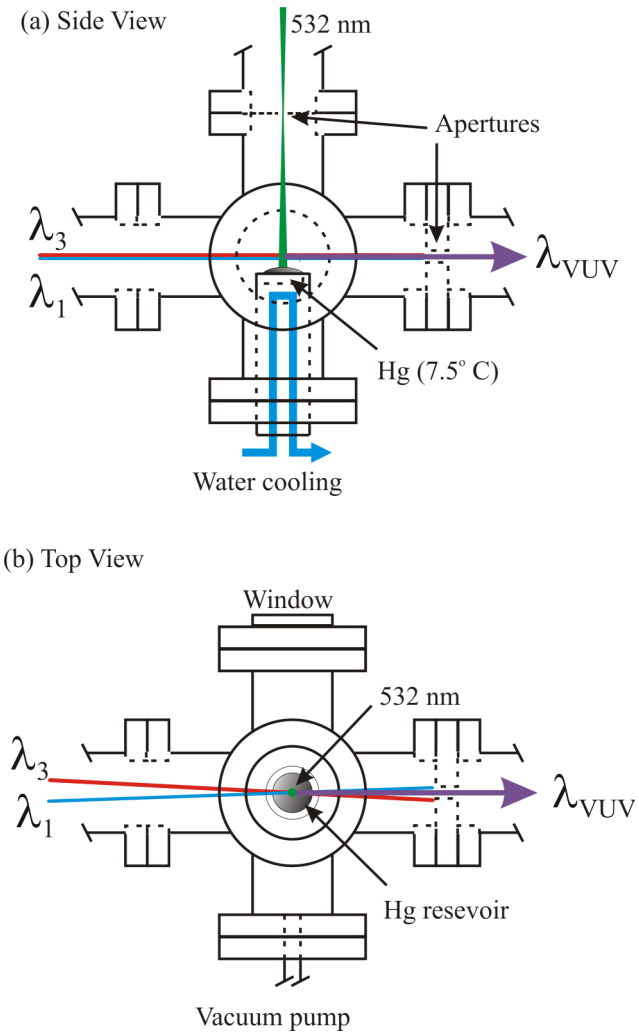

FIG. 3. Schematic of the ablation mixing cell. (a) side view and (b) top view.

by a beam diameter (~2 mm) at the photoionization region located 35 cm from the lens, the 312.85 nm and 625 nm beams must be translated at 2 and 8 mm from the center of the lens, respectively. However, for mixing 312.85 nm and 312 nm beams, the beams needed to be translated are 2 and 4 mm, respectively, from the center of the lens to produce the same separation between the 312.85 nm and VUV beams. In practice, the angles employed in this work were chosen in order to minimize the background from 104 nm radiation (discussed below) while being limited by the physical dimensions of the achromatic lens. The optimal interaction angle for a given setup will depend on the wavelengths of the input lasers, VUV wavelength, and physical limitations of the experimental apparatus.

The VUV beam direction will change slightly as λ_3 is scanned. Across the tuning range of a typical laser dye for λ_3, the change in VUV photon energy is less than 3%, leading to small changes in VUV pointing direction. For example, scanning λ_3 from 610 nm to 660 nm, the angle through which the VUV beam moves is 0.02°(0.13 mm when measured 35 cm from the focal point). The effect of this small change in VUV pointing direction was not significant in our experiments. If the VUV propagation distance is significantly longer, the wavelength dependence of the VUV propagation angle could become important.

The VUV beam intensities were monitored by photoionization of various gases with well-established ionization energies (I.E.) and photoionization cross sections.[37] The propene (I.E. = 9.7 eV), acetylene (I.E. = 11.4 eV), and 1-butene (I.E. = 9.6 eV) beams were produced by a piezoelectrically operated pulsed valve. Photoions were detected using either a Wiley-McLaren time-of-flight mass spectrometer or by collection using two stainless steel plates, one held at + 50 V and the other connected to a digital oscilloscope (terminated 50 Ω to ground) where the signal was read as a time dependent voltage. Absolute VUV intensities were calculated using the density of the molecular beam, photoionization cross section, and oscilloscope signal with the voltage integrated over the pulse width. The detection efficiency was calibrated in a separate series of experiments at 125 nm using a slow flow of a gas into the chamber at measured total pressure. After the absolute VUV intensity had been calculated at 125 nm, it was possible to use the absolute signal level at a given mass in the TOF spectrum to compare between different schemes under the same TOF conditions, i.e., the same microchannel plate voltage, ion optics setting, and molecular beam conditions. The different photoionization cross sections were used to compare VUV and XUV intensities at different wavelengths.[37,38] For schemes producing high VUV intensities, the TOF peaks were sometimes distorted due to space-charge effects, making intensity measurements impossible. In these cases, we either used the two-plate detection method using the same molecular beam, or decreased the concentration of gas in the molecular beam.

Absolute measurements of VUV and XUV intensities are difficult. We estimate the uncertainty in absolute VUV intensity at 125 nm to be ±50%. The VUV and XUV intensities reported at 121 nm, 112 nm, and 104 nm have been calculated based on signal levels relative to that at 125 nm. These measurements are subject to the same systematic error as the 125 nm VUV, with a further ±10% uncertainty for each of these measurements (±55% overall). Intensities for shorter wavelengths have been calculated in a similar manner relative to 104 nm intensity, inducing a further ±10% uncertainty (±60% overall).

The 532 nm output of a second Nd:YAG laser (Continuum NY 81-10 or Surelite II) was used for Hg vaporization. A half wave plate and polarizer were used to adjust the pulse energy without affecting the spatial beam profile. The laser was focused 8 cm above the Hg surface using a 40 cm focal length lens, producing a spot diameter of approximately 2 mm on the Hg surface. In order to prevent Hg vapor from reaching the ablation laser input window, the ablation laser was focused through a plate with a 2 mm hole drilled through it, located at the focal point of the laser. Figure 3 shows the configuration of the ablation cell. The timing and alignment of the ablation laser were critical for optimal VUV generation; the Hg density in the mixing region is affected by both the ablation laser pulse energy and the delay time between the ablation laser and the UV and visible lasers. The optimal delay was varied using an SRS DG535 digital delay generator. Typically, the ablation laser was triggered 5-20 μs before the UV and visible dye lasers.

When the 312.85 nm laser was well overlapped both spatially and temporally with the Hg plume, bright blue fluorescence was visible at the 312.85 nm focus. This fluorescence was most likely due to the fluorescence from $7^1S_0 \rightarrow 6^3P_1$ at 407.8 nm[39] and was not visible if the 312.85 nm laser wavelength was detuned or the timing between the dye lasers and the ablation laser was not optimal. The presence of the blue fluorescence was a useful visible check for correct alignment, wavelength, and timing.

A simple and versatile configuration facilitates convenient access to photon energies of 9.9 eV, 11.0 eV, and 11.9 eV without the need for any dye changes. One DCM dye laser was used to produce light at $\lambda = 312.85$ nm. The second DCM laser generated 625 nm radiation to produce 9.9 eV photons. To obtain 11.0 eV photons, 650 nm radiation (produced using the same DCM dye) was mixed with the 1064 nm output of the unseeded Nd:YAG laser, yielding 403 nm radiation, which was subsequently mixed with the 312.85 nm laser. Finally, 11.9 eV photons were produced by either tripling the output of the 312.85 nm laser in a collinear geometry or by mixing the 312.85 nm laser with the doubled output (~312 nm) of the second DCM dye laser in a noncollinear geometry.

III. RESULTS/DISCUSSION

A. Phase matching conditions

In most of the previous studies employing Hg as the nonlinear medium,[9,10] tight-focusing conditions were employed. The dimensionless phase matching factor, $F'(b\Delta k)$, for tight-focused fundamental beams in heated cells has been discussed in detail.[9,10,40] Briefly, phase matching in a tightly focused configuration where $b \ll L$ (the confocal parameter is shorter than the length of the nonlinear mixing medium, as in the case of our heated Hg cell), is described by

$$F'(b\Delta k) = \begin{cases} (\pi b\Delta k)^2 e^{b\Delta k}, & \Delta k < 0 \\ 0, & \Delta k \geq 0 \end{cases}, \quad (1)$$

where b is the confocal parameter and Δk is the phase mismatch between the fundamental and generated radiation, defined as

$$\Delta k = 2\pi[2(n_4 - n_1)\lambda_1^{-1} + (n_4 - n_3)\lambda_3^{-1}], \quad (2)$$

with n_i being the refractive indices of the respective wavelengths, λ_i.

The situation using a laser vaporization cell for producing the nonlinear medium is similar to the phase matching condition found in pulsed jet mixing experiments, where the condition $b \ll L$ is not necessarily true, i.e., the confocal parameter of the focused laser beam is *not* much shorter than the length of the mixing medium. Rettner *et al.*[22] suggest that in the case of focusing near a pulsed jet, the phase matching conditions are close to those in plane-wave mixing. In such a case, $F'(b\Delta k)$ would take the form

$$F'(b\Delta k) = [(2L/b)\frac{\sin(\Delta kL/2)}{(\Delta kL/2)}]^2. \quad (3)$$

As a result, optimal phase matching is not limited to regions of negative dispersion, making the addition of negatively dispersive gases for phase matching purposes unnecessary.[22,24] For VUV generation in Hg, it is well-know that VUV can be generated on the high energy side of the atomic resonance, in addition to the low energy side.[9,10]

Phase matching conditions for noncollinear alignment of the fundamental beams at a small angle, θ, have been discussed previously.[26,27,41] The effect of noncollinear alignment of the fundamental beams is evident in the phase mismatch (Δk) term of the phase matching factor, $F'(b\Delta k)$. In the case of $\lambda_1 = \lambda_2 = 312.85$ nm, an additional term is needed for Δk,

$$\Delta k_{cross} = \frac{k_1 k_3}{2k_1 + k_3}\theta^2. \quad (4)$$

Thus, introducing noncollinearity will change the optimal range and peak wavelength for sum-frequency mixing, as has been demonstrated both theoretically and experimentally.[26,41]

B. Ablation laser conditions and timing

The VUV intensities are strongly dependent on the timing of the ablation laser relative to the dye lasers. For 9.9 eV generation (mixing 312.85 nm and 625 nm), the maximum VUV intensities were observed for ablation laser pulse energies of 9 mJ triggered 18 μs before the dye lasers. However, for decreasing ablation laser pulse energies, the optimal delay between the ablation laser trigger and the dye lasers trigger decreased. For example, the optimum time from the ablation trigger to the dye laser trigger was only 4 μs using ablation pulse energies of ~2 mJ. In general, for less efficient schemes producing lower VUV pulse intensities, the maximum VUV intensities were observed with shorter delays between the ablation laser trigger and dye laser trigger. For example, the optimum delay was ~7 μs for 121 nm and 112 nm generation. For tripling 312.85 nm to make 104.3 nm, optimal delay was ~5 μs. For a given VUV wavelength, the optimal ablation laser timing was found to be the same for both collinear and noncollinear geometries. The mercury vapor density in the plume was not measured directly, but is assumed to be similar to the density of 5×10^{16} atoms/cm^3 estimated by Chénais *et al.* in their experiment.[33] Atomic densities in heated cells are also typically 10^{16}-10^{17} atoms/cm^3.

C. Schemes employing the 7 $^1S_0$ two-photon resonance

1. 9.9 eV (125 nm)

When λ_3 is tuned to 623.6 nm, the 9 $^1P_1$ resonance (79 963.85 cm^{-1})[42] is accessible for resonance enhancement. The efficiency for VUV generation near 125 nm using the ablation cell is compared to that for the heated cell in Fig. 4. The usable VUV intensity employing the ablation cell is about 80% of that using the heated cell. However, the tuning curves near the 9 $^1P_1$ resonance differ considerably. For the heated cell, the shape of the tuning curve is in good agreement with previously observed tuning curves.[9,10] The resonance enhancement near the 9 $^1P_1$ resonance using ablation is much broader than using the heated cell. Also, when using the ablation cell, the VUV intensity does not decrease as sharply

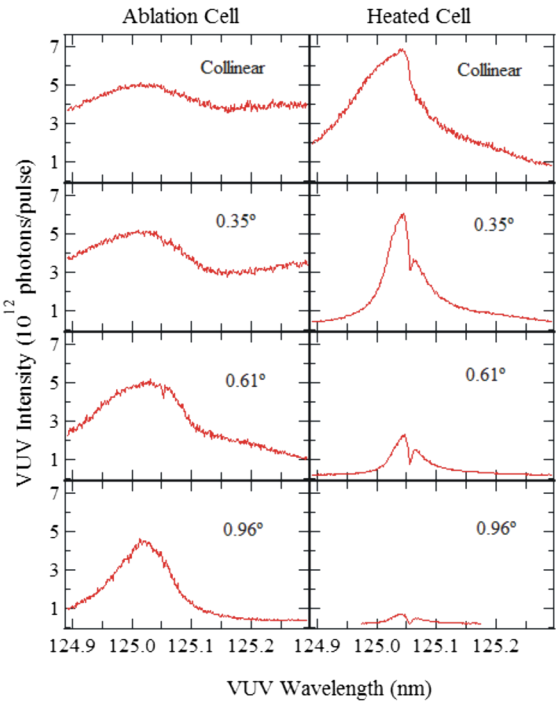

FIG. 4. Tuning curves around the 9 $^1P_1$ resonance (5.5 mJ/pulse @ 312.85 nm, 5 mJ/pulse @ 625 nm, 7.5 mJ/pulse @ 532 nm).

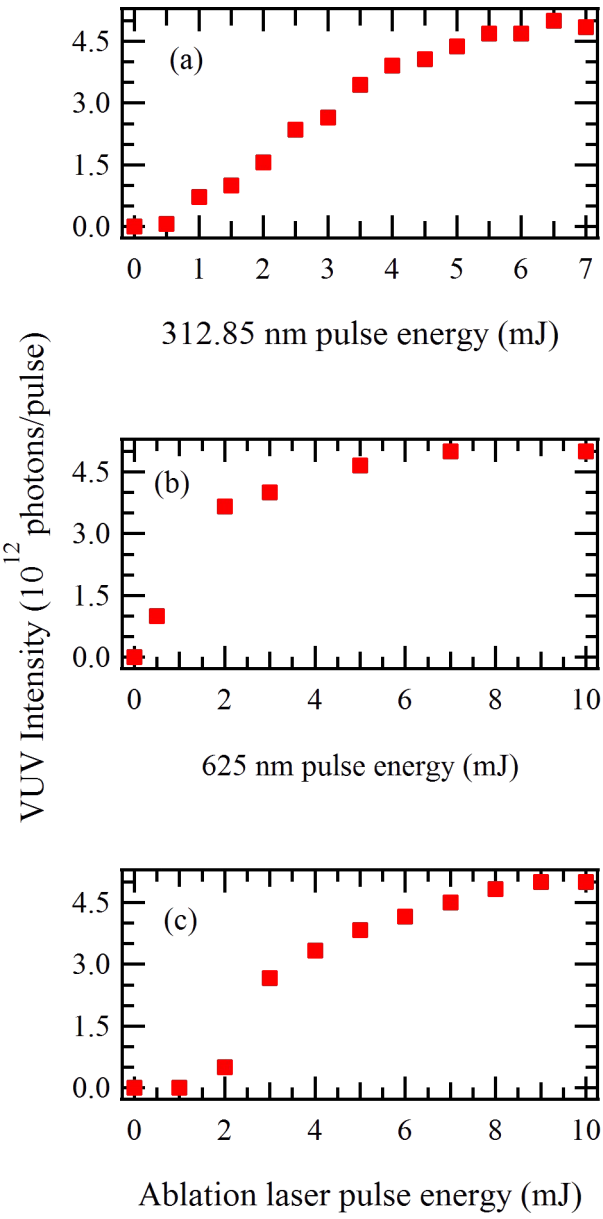

FIG. 5. VUV intensity vs. (a) 312.85 nm pulse energy (5 mJ/pulse @ 625 nm, 7.5 mJ/pulse @ 532 nm), (b) 625 nm pulse energy (5.5 mJ/pulse @ 312.85 nm, 7.5 mJ/pulse @ 532 nm), (c) ablation laser pulse energy (5.5 mJ/pulse @ 312.85 nm, 5 mJ/pulse @ 625 nm). The ablation laser was triggered 12 μs before the UV and visible lasers.

with increasing the crossing angle as in the heated cell. The use of a window in the heated cell reduces photon flux by about 20% at 125 nm. Thus the ablation cell produces about 65% as many VUV photons as the heated cell at 125 nm. However, the number of usable photons produced is the quantity of practical interest. Consequently, VUV intensities are described in terms of "usable photons" rather than the absolute number of photons produced per pulse in the case of the heated cell. In the ablation cell, since no window is required, "usable photons" and "absolute photons" are the same. Using the two-plate detector, we calculate 5×10^{12} photons/pulse near 125 nm under optimal collinear conditions with the ablation cell. This is about an order of magnitude smaller than we produce using collimated lasers in a 1 m long Hg cell.[11]

Chénais *et al.* reported the dependence of the "enhancement ratio," defined as the ratio of the VUV intensity with the vaporization laser on relative to that with the vaporization laser off, as a function of UV, visible, and ablation laser beam pulse energies.[29] We have carried out similar experiments but instead report the relative intensity of the VUV generated as functions of the three input laser pulse energies, shown in Fig. 5. Figure 5(a) shows a linear dependence on 312.85 nm pulse energy up to ~4.5 mJ/pulse, after which the VUV intensity begins to plateau. Figure 5(b) shows that the VUV intensity begins to level off at even lower 623.6 nm pulse energies. For the ablation laser, there is a low energy threshold, below which little or no VUV is generated as seen in Fig. 5(c). Above this VUV, intensity increases with input pulse energies up to ~9 mJ/pulse. The VUV intensity does not increase significantly with further increases in ablation laser pulse energy. Chénais *et al.* attribute this effect to laser energy being shielded by the generated plasma, termed "plasma shielding."[33,43]

At high ablation pulse energies (>10 mJ/pulse), we observed buildup of liquid Hg on entrance windows to the cell. However, at ablation laser pulse energies of 7 mJ/pulse or less, no Hg buildup was observed even after >100 h of operation. As shown in Fig. 5, the VUV pulse intensities plateau at lower pulse energies than in the standard heat pipe configuration in either a focused or unfocused geometry.[9,11,13] To date we have not studied the effect of using achromatic focusing lenses with different focal lengths. Since VUV conversion efficiencies can be high even using unfocused lasers (2 mm dia. beam), it is likely that higher VUV intensities using an ablation source could be produced using higher input pulse energies and a larger beam waist produced by a longer (e.g., 50-60 cm) focal length lens.

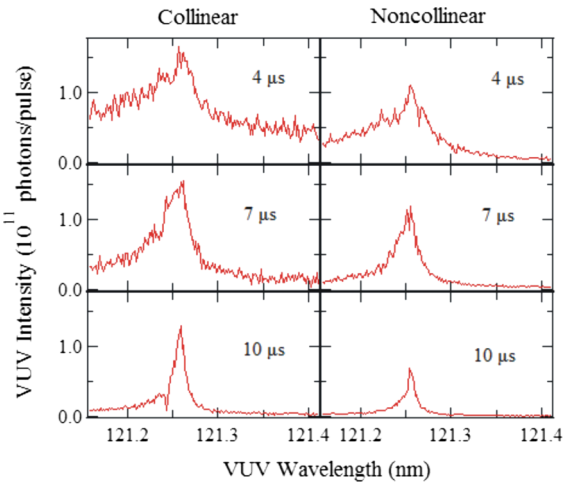

FIG. 6. Left: collinear scans, ablation laser triggered 4, 7, and 10 μs before the UV and visible lasers (top to bottom). Right: 0.59° crossing angle with same ablation laser timing. Laser pulse energies: 2.0 mJ @ 312.85 nm, 2.0 mJ @ 540 nm, and 7 mJ of 532 nm ablation.

2. 10.2 eV (121.3 nm)

Tuning λ_3 near $\lambda = 539.5$ nm accesses the 12 $^1P_1$ state at 82 463.9 cm^{-1} (121.3 nm).[37] We measured 2×10^{11} photons/pulse at this VUV wavelength. The decrease in efficiency upon tuning to higher energy resonances has been reported previously by Hilbig and Wallenstein and Mahon and Tomkins.[9,10] Tuning curves around the 12 $^1P_1$ resonance are shown in Fig. 6. The curves on the left side employed collinear input beams; the tuning curves on the right side were recorded using a crossing angle of 0.59°. The shapes of the tuning curves were affected by the delay between Hg vaporization and VUV pump beams and by the crossing angle of the two incident laser beams. For longer delays between the ablation and VUV lasers, the tuning curve peaks more sharply near the 12 $^1P_1$ resonance. Also, as seen in the case of the 9 $^1P_1$ resonance, the conversion efficiency decreases and the resonance enhancement becomes more sharply peaked for noncollinear geometries.

The constant contribution from the signals resulting from frequency tripling of the 312.85 nm beam (producing 104.3 nm light, as discussed below) has been subtracted from the data shown in Fig. 6. This background was most prevalent using collinear beams and short delays between ablation laser and dye laser triggers. At short ablation laser delay times and collinear alignment, the propene photoionization signal from 104.3 nm light was ~35% of the signal produced using two input beams (121.3 nm). For longer delays between ablation laser and dye laser triggers and employing a noncollinear geometry, the 104.3 nm background contribution was typically ~3%.

Figure 7 illustrates how intensities at 121.3 nm varied with input laser pulse energies, with the ablation laser triggered 7 μs before the input laser beams. As the 312.85 nm laser pulse energy was increased, the VUV intensity began to plateau above 1.0 mJ/pulse. On the other hand, a linear dependence was observed for the 540 nm laser up to 4.0 mJ/pulse. As was seen for the generation of VUV at 125 nm, the plot of VUV intensity vs. ablation laser pulse energy shows a threshold below which very little VUV was generated. Over the interval

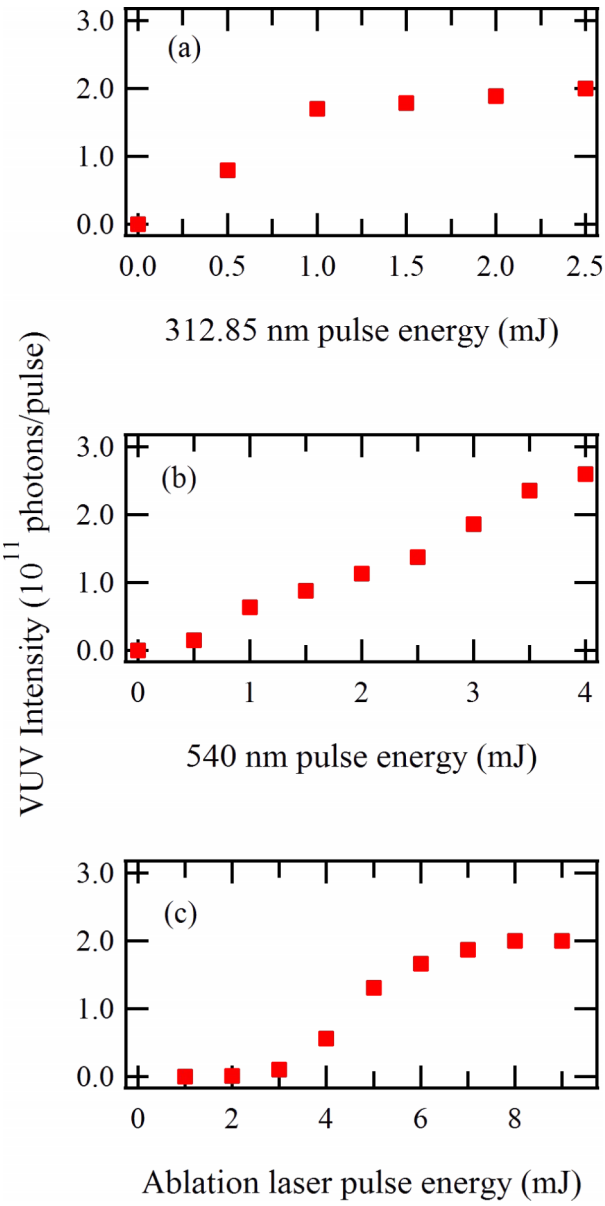

FIG. 7. VUV intensity vs. (a) 312.85 pulse energy (2.5 mJ/pulse @ 540 nm, 6.5 mJ/pulse @ 532 nm), (b) 540 pulse energy (2.5 mJ/pulse @ 312.85 nm, 6.5 mJ/pulse @ 532 nm), (c) ablation laser pulse energy (2.5 mJ/pulse @ 312.85 nm, 2.5 mJ/pulse @ 540 nm). The ablation laser was triggered 7 μs before the UV and visible lasers.

ranging from 3 to 6 mJ/pulse, a relatively linear dependence was observed, reaching a plateau near 8 mJ/pulse.

Pulsed radiation at the Hydrogen Lyman-α (121.6 nm) transition is close in energy to the VUV generated by this scheme, and has been the focus of many previous studies.[1,3,6,7] Nonlinear mixing mediums *other than mercury* (most notably Kr with Ar for phase matching) have been used to generate up to 4.3×10^{12} photons/pulse.[7,44] Even when accounting for losses due to optical elements, schemes employing rare gases provide higher intensity at Lyman-α than our ablated Hg source.[7] Hg has previously been used as a nonlinear mixing medium for generating *continuous* VUV at 121.6 nm, yielding 3×10^8 photons/s.[8] Eikema *et al.* used 257 nm and 399 nm lasers to reach the 7 $^1S_0$ resonance in Hg, similar to the method we describe below, and then 545 nm to produce 121.6 nm,

radiation (Lyman- α). They also produced 121.6 nm using two photons at 280 nm to reach the 6 ^{1,3}D resonances and a third photon at 915 nm utilizing the 12 $^1P_1$ resonances in Hg.

3. 11.0 eV (112 nm)

Using the 7 $^1S_0$ two-photon resonance, λ_3 ~403 nm produces VUV wavelengths near 112 nm (~88 700 cm^{-1}). According to the NIST atomic database, the 5d^9 6s^2($^2D_{3/2}$) 6p $^2[1/2]_1$ state lies at 88 759.6 cm^{-1}.[42] Since this lies above the Hg ionization limit, no sharp peak is present, although some enhancement is observed in the vicinity of the resonance. With the available laser pulse energies (3 mJ/pulse at 312.85 nm, 5 mJ/pulse at 403 nm), 2×10^{11} photons/pulse was measured at 112 nm. Higher input pulse energies would likely increase the VUV intensities in this energy range. Figure 8 shows the dependence of the VUV intensity on input pulse energies. The dependence on the 403 nm laser pulse energy is linear, suggesting that high pulse energies would lead to increased VUV intensities. As before, a lower limit is seen for the ablation laser pulse energy, as well as a plateau above 6 mJ/pulse.

An alternative method for reaching energies near 88 700 cm^{-1} utilizes the single photon resonance enhancement afforded by the 6 $^3P_1$ state at 253.7 nm. In this case, a photon near 408 nm reaches the same 7 $^1S_0$ two-photon resonance as two photons at 312.85 nm. The third photon for four-wave mixing can be either a second 253.7 nm or 408 nm photon to give 12.8 eV or 11 eV VUV, respectively. Tuning very close to the 253.7 nm resonance results in strong absorption by Hg, leading to decreased VUV generation. However, tuning to either side of the 253.7 nm resonance results in increased VUV intensities, with the maximum VUV observed 30 cm^{-1} to 200 cm^{-1} below the 6 $^3P_1$ state, corresponding to λ_1 ~ 254 nm. Using 0.8 mJ/pulse at 254 nm and 4.5 mJ/pulse at 408 nm, two different wavelengths were produced, 96.9 and 113 nm, corresponding to photon energies of 12.8 and 11 eV. By photoionizing a molecular beam of acetylene (ionization energy of 11.4 eV), we measured the intensity of the 96.9 nm VUV to be 2×10^8 photons/pulse. When observing a molecular beam of 1-butene, we measured the total VUV intensity to be 5×10^{11} photons/pulse, leading to the conclusion that generation of 113 nm photons is more than three orders of magnitude, more efficient than generation of 96.9 nm photons. Figure 9 shows VUV intensity vs. 254 nm, 408 nm, and 532 nm pulse energies.

Hilbig and Wallenstein have previously demonstrated VUV generation in this wavelength range, both by nonresonant sum-frequency mixing in krypton leading to 114 nm VUV, and by using the 6 $^1S_0$–6 $^1D_2$ two-photon resonance in mercury to generate 112 nm VUV. The VUV intensities produced were 1×10^{10} and 5×10^{11} photons/pulse, respectively.[2,9] Accounting for the transmission of one LiF optic in this wavelength range (<50%), their maximum usable VUV intensities were 5×10^9 and 2.5×10^{11} photons/pulse.

4. 11.9 eV (104 nm)

By tripling the 312.85 nm radiation, 11.9 eV photons (104.3 nm, 95 892 cm^{-1}) were produced with quite high efficiencies even though the nearest known resonance (5d^{10}6p^2 $^3P_2$) lies at 96 190 cm^{-1}, i.e., 300 cm^{-1} away.[42] Alignment of two 312.85 nm beams with a crossing angle of 0.67° resulted in intensities approximately half than using the collinear geometry. By generating the second 312 nm beam with a second dye laser, we scanned λ_3 and looked for resonance enhancements, but none were observed. The maximum absolute intensity of this scheme under collinear conditions was 4×10^{10} photons/pulse. Production of VUV at 104.3 nm has been observed previously, but intensity measurements were either not reported,[10,19] or VUV was generated in a heated cell with no window connected directly to a detector under a few Torr of He,[10] in which case Mahon and Tomkins measured 4×10^{10} photons/pulse under tight focusing conditions. Kwon *et al.* measured the VUV intensity for mixing two photons at 312.85 nm and a third photon

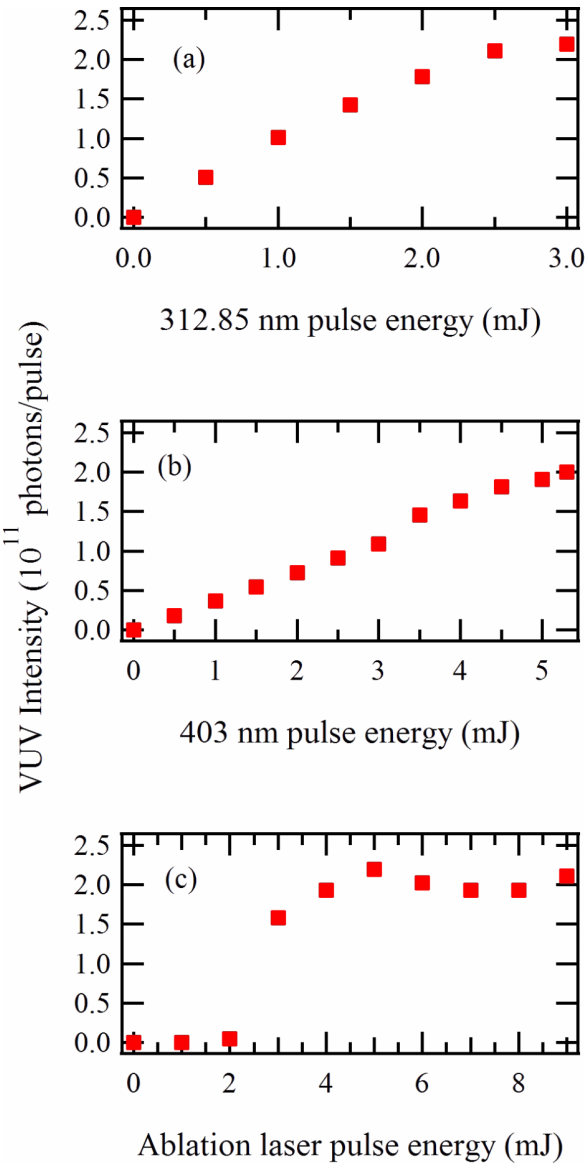

FIG. 8. VUV intensity vs. (a) 312.85 nm pulse energy (5.5 mJ/pulse @ 403 nm, 6.5 mJ/pulse @ 532 nm), (b) 403 nm laser (3.0 mJ/pulse @ 312.85 nm, 6.5 mJ/pulse @ 532 nm), and (c) ablation laser pulse energy (3.0 mJ/pulse @ 312.85 nm, 5.5 mJ/pulse @ 403 nm). The ablation laser was triggered from 5 to 9 μs before the UV and visible lasers.

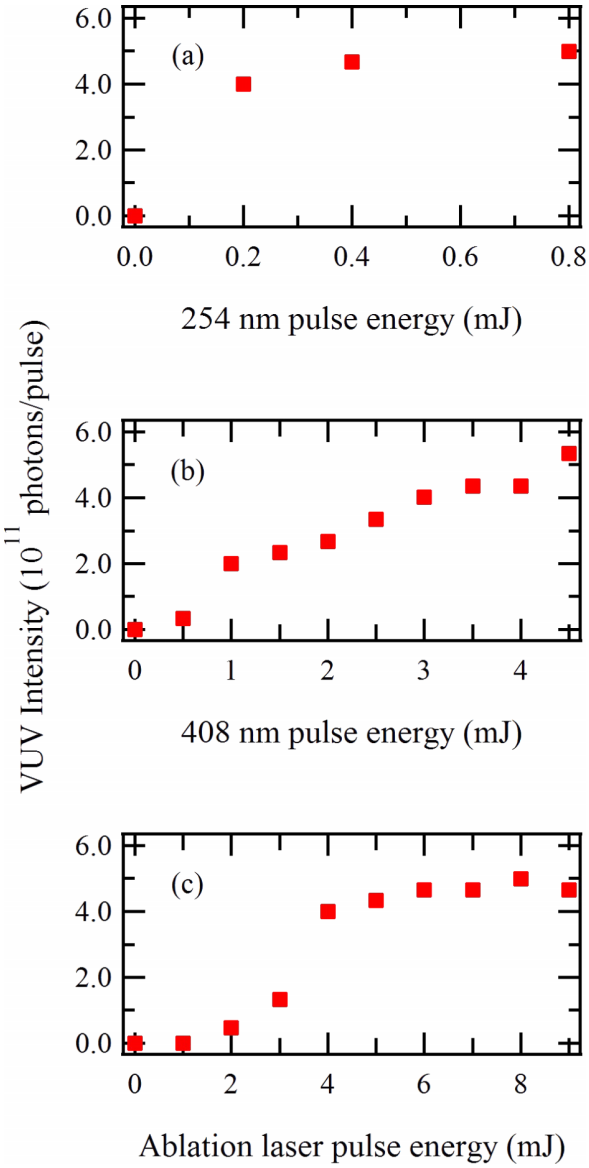

FIG. 9. VUV intensity vs. (a) 254 nm laser pulse energy (4.5 mJ/pulse @ 408 nm, 6.5 mJ/pulse @ 532 nm), (b) 408 laser pulse energy (0.8 mJ/pulse @ 254 nm, 6.5 mJ/pulse @ 532 nm), and (c) ablation laser pulse energy (0.8 mJ/pulse @ 254 nm, 4.5 mJ/pulse @ 408 nm). The ablation laser was triggered 14 μs before the UV and visible lasers.

ranging from 320 to 355 nm and reported a usable photon intensity of 4×10^9 photons/pulse.[19] Marinero *et al.* report 7×10^9 photons/pulse from 100 to 102.3 nm by frequency tripling in a pulsed Ar gas source.[45] Cromwell *et al.* reported XUV peak intensities of $>10^{11}$ around 98 nm when using resonance enhanced mixing of a pulsed amplified ring laser in a pulsed beam of Ar.[24] This XUV intensity is similar to the maximum 104 nm intensity, we were able to generate using commercial dye lasers when the Hg mixing region volume was increased, as discussed below.

Figure 10 shows 104 nm intensities as a function of input laser pulse energies in collinear geometry. Figure 10(a) shows a clear saturation above 2 mJ/pulse for the input 312 nm power, similar to the trends observed in both 125 nm and 121 nm generation. As seen in Fig. 10(b), for 104 nm production, a threshold is observed for the ablation laser pulse energy

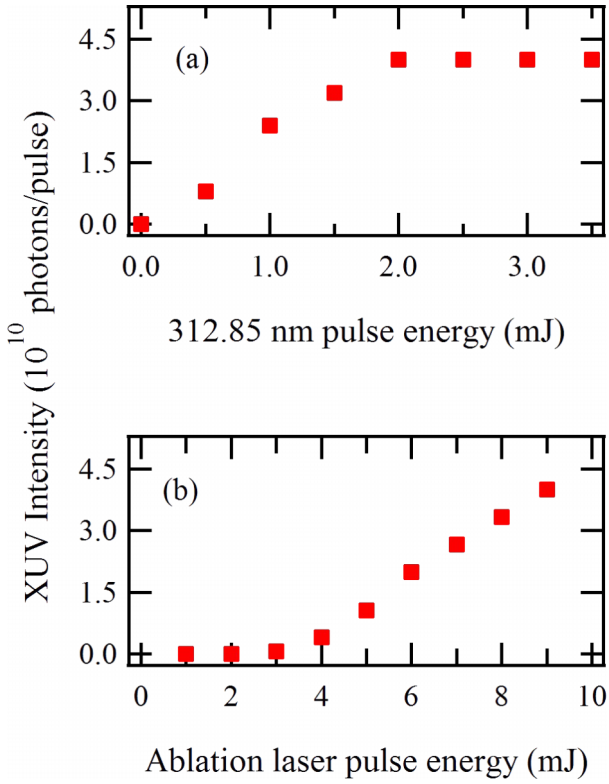

FIG. 10. VUV intensity vs. (a) 312.85 nm laser pulse energy (6.5 mJ/pulse @ 532 nm), and (b) ablation laser pulse energy (2.5 mJ/pulse @ 312.85 nm). The ablation laser was triggered 5 μs before the 312.85 nm laser.

followed by a liner VUV intensity increase. We observed no plateau in 104 nm intensity for high ablation laser pulse energies.

D. Schemes employing the 8 $^1S_0$ two-photon resonance

1. 13.8 eV (89.6 nm)

The 8^1S_0 resonance in Hg lies at 74 404 cm^{-1}, accessible by two photons at 268.8 nm.[38] There have been a number of previous studies employing this resonance.[18,20,46] Using a collinear geometry, tripling of the 268.8 nm laser was first optimized, producing light at 89.6 nm (13.8 eV). We found that the XUV intensity at this wavelength is about three orders of magnitude weaker than at 104.3 nm (the analogous scheme using 7^1S_0), i.e., we produced 3×10^7 photons/pulse at 89.6 nm. This is about an order of magnitude greater than that reported by Herman and Stoicheff.[20] Hannemann *et al.* describe generating 91 nm XUV using four-wave mixing in Kr, while they did not measure the XUV intensity directly, they estimated 10^9 photons/pulse.[27] Koudoumas and Efthimiopoulos estimated 10^8 photons/pulse generated at this wavelength, but transmission from their mixing region to their detection region was ~5%, i.e., their usable VUV intensity was $\sim 5 \times 10^6$ photons/pulse.

2. 11.0 eV (112 nm)

By employing the 268.8 nm two-photon resonance and adding $\lambda_3 \sim$ 620-710 nm, we observed a large enhancement

in VUV production (relative to tripling 268.8 nm to produce 89.6 nm radiation), with no strong dependence on the exact wavelength of λ_3. The use of $\lambda_3 \sim 695$ nm produces VUV photons near 11 eV, similar to the scheme involving the 7S resonance employing 312.85 nm + 403 nm input beams. We found that the VUV intensities near 11 eV using the 8 $^1S_0$ state to be 10^{10} photons/pulse, a factor of 15-20 smaller than generating the same wavelength using the 7 $^1S_0$ two photon resonance.

E. Schemes employing the 9 $^1S_0$ two-photon resonance

1. 14.6 eV (85 nm)

Two photons at 255.1 nm are resonant with the 9 $^1S_0$ state in Hg, which lies at 78 404.24 cm^{-1}.[42] This two-photon resonance represents another potential route to production of XUV photons using λ_3 in the visible and near-UV. Using 0.7 mJ/pulse at 255.1 nm, 6×10^6 photons/pulse were generated by tripling 255.1 nm to give 85 nm (14.8 eV/photon). Our laser system was not optimized for production of light at 255.1 nm. Since much higher input pulse energies near 255.1 nm could be produced (>3 mJ), at least an order of magnitude with greater XUV intensities in the 14.6 eV range should be easily achievable.

F. Refocusing using concave silicon mirror

The use of focused input lasers produces divergent VUV and XUV output beams. However, some applications require that the VUV or XUV beam be refocused, this requiring the use of reflective optics at wavelengths shorter than 104 nm. According to the calculations by Hunter,[47] the reflectivity of silicon at normal (90°) incidence exceeds 60% in the VUV and XUV regions. We have carried out experiments using a 1 in. diameter Si infrared lens (1 m radius of curvature) as a mirror at near-normal incidence in order to recollimate 112 nm light produced by noncollinear mixing of 312.85 and 404 input beams. Consistent with the calculations, the near-normal reflectance was about 60% at 112 nm. Since highly polished Si lenses and mirrors can be obtained at relatively low cost (e.g., ISP Optics), their use provides a very simple and cost-effective approach for refocusing or recollimating VUV and XUV laser beams.

G. The effect of increased beam diameter

By using a longer focal length lens for focusing the input beams, the radius of the beam waist, ω_0, is increased according to the relationship $\omega_0 = \left(\frac{4\lambda}{\pi}\right)\left(\frac{f}{d}\right)$, where f is the focal length, d is the laser beam diameter before the lens, and λ is the wavelength. This consequently increases the mixing volume. Using input pulse energies of 7 mJ at 312.85 nm, by replacing the 34 cm focal length achromat with a 53 cm focal length lens, the λ = 104 nm XUV intensity doubled to 7×10^{10} photons/pulse. However, after making the same change for production of light at λ = 125 nm (using 7 mJ at 312.85 nm + 11 mJ at 623.6 nm), the output pulse energy decreased, most likely due to the poor spatial overlap resulting from the use of a nonachromatic lens.

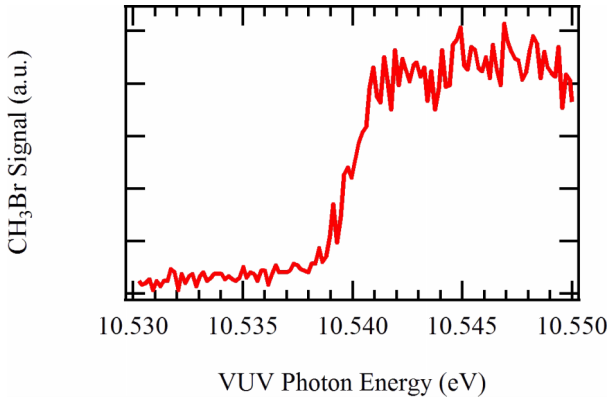

FIG. 11. Photoionization threshold of CH_3Br, where λ_3 is scanned from 472.7 to 476.7 nm. The observed ionization threshold of 10.539 eV is within the uncertainty of the accepted value of 10.541 ± 0.003 eV.

H. Ablation of a line

In an effort to increase the length of the mixing region, we replaced the spherical lens focusing the ablation laser with a 25 cm focal length cylindrical lens. This allowed ablation of a 1 mm × 10 mm line of mercury rather than a 2 mm dia. spot. Using this configuration, we tested both 104 nm and 125 nm generations. Intensity at 104 nm was about 20% greater (9×10^{10} photons/pulse) using the cylindrical lens compared to that using the 40 cm FL spherical lens. At 125 nm, the VUV intensity decreased by a factor of two, likely because the 53 cm FL lens was not achromatic. However, the power dependences of both the 312.85 nm and 623.6 nm radiation were linear at pulse energies up to 7 mJ/pulse at 312.85 nm and 11 mJ/pulse at 623.6 nm. These results suggest that higher pulse energies, a cylindrical lens for ablation, and an achromatic lens for the input beams, could lead to increased VUV intensities.

I. Photoionization threshold of CH_3Br

We have tuned the VUV source to the photoionization threshold of methyl bromide, CH_3Br, which has a well established ionization energy of 10.541 ± 0.003 eV.[48] Using noncollinear mixing of 312.85 nm photons with 474.7 nm photons, the observed appearance energy of CH_3Br^+ observed by photoionization of a molecular beam containing 0.5% CH_3Br in He was within the currently accepted range (Fig. 11).

IV. CONCLUSIONS

We have developed and characterized an approach for generating VUV and XUV radiation by resonance enhanced four-wave sum-frequency laser mixing in laser vaporized Hg. Noncollinear mixing makes it possible to eliminate all optical elements following VUV or XUV generation, facilitating windowless operation with spatial separation of the beams. Compared to the use of heated Hg cells, the use of laser vaporization also leads to broader tuning curves due to less restrictive phase matching conditions near Hg atomic reso-

nances. We have produced radiation in the 9.9 eV–14.6 eV range, and highlighted a convenient approach allowing rapid access to three different wavelengths corresponding to photon energies of 10, 11, and 12 eV.

The usable VUV intensities we have generated at various wavelengths, particularly for photon energies >11 eV, are in most cases greater than the usable photon intensities demonstrated previously. Near 11 eV, we measured a factor of two greater usable photon intensity (5×10^{11} photons/pulse).[9] At 104 nm (12 eV), our usable VUV intensity of 9×10^{10} photons/pulse, is similar to a previous estimate of $\sim 10^{11}$ photons/pulse using a much more complex laser system.[24] At 89.6 nm (13.8 eV), we generated an order of magnitude more VUV than previously measured using Hg as a nonlinear mixing medium at that wavelength.[20]

The Nd:YAG pumped dye laser system employed in this work is very modest by present-day standards. Using more modern commercially available pulsed lasers, input pulse energies >10 times higher than those used here are readily achievable. Therefore, with some effort, much higher pulse energies in the VUV and XUV are readily achievable using the methods described here.

ACKNOWLEDGMENTS

This research was supported by the U.S. Department of Energy, under Grant No. DE-FG02-00ER15095 (Free Radical Chemistry), and by the National Science Foundation, No. CHE-1301156 (Halogen Oxide Chemistry).

[1]J. W. Hepburn, "Applications of coherent vacuum ultraviolet to photofragment and photoionization spectroscopy," in *Vacuum Ultraviolet Photoionization and Photodissociation of Molecules and Clusters*, edited by C. Y. Ng (World Scientific, Singapore, 1991), pp. 435–485.
[2]R. Hilbig and R. Wallenstein, Appl. Opt. **21**, 913 (1982).
[3]R. Mahon, T. J. McIlrath, V. P. Myerscough, and D. W. Koopman, IEEE J. Quantum Electron. **15**, 444 (1979).
[4]K. S. E. Eikema and W. Ubachs, in *Handbook of High Resolution Spectroscopy*, edited by M. quack and F. Merkt (John Wiley & sons, 2010), pp. 1374–1413.
[5]R. Hilbig and R. Wallenstein, IEEE J. Quantum Electron. **19**, 194 (1983).
[6]H. Langer, H. Puell, and H. Roehr, Opt. Commun. **34**, 137 (1980).
[7]J. P. Marangos, N. Shen, H. Ma, M. H. R. Hutchinson, and J. P. Connerade, J. Opt. Soc. Am. **7**, 1254 (1990).
[8]K. S. E. Eikema, J. Walz, and T. W. Hänsch, Phys. Rev. Lett. **83**, 3828 (1999).
[9]R. Hilbig and R. Wallenstein, IEEE J. Quantum Electron. **19**, 1759 (1983).
[10]R. Mahon and F. S. Tomkins, IEEE J. Quantum Electron. **18**, 913 (1982).
[11]D. R. Albert, D. L. Proctor, and H. F. Davis, Rev. Sci. Instrum. **84**, 063104 (2013).
[12]A. V. Smith and W. J. Alford, J. Opt. Soc. Am. B **4**, 1765 (1987).
[13]C. H. Muller III, D. D. Lowenthal, M. A. DeFaccio, and A. V. Smith, Opt. Lett. **13**, 651 (1988).
[14]W. A. VonDrasek, S. Okajima, and J. P. Hessler, Appl. Opt. **27**, 4057 (1988).
[15]R. R. Smardzewski, Appl. Spectrosc. **31**, 332 (1977).
[16]T. B. Lucatorto, T. J. McIlrath, and J. R. Roberts, Appl. Opt. **18**, 2505 (1979).
[17]L. Hellner and J. Lukasik, Opt. Commun. **51**, 347 (1984).
[18]E. Koudoumas and T. Efthimiopoulos, Laser Chem. **13**, 129 (1993).
[19]C. H. Kwon, H. L. Kim, and M. S. Kim, Rev. Sci. Instrum. **74**, 2939 (2003).
[20]P. R. Herman and B. P. Stoicheff, Opt. Lett. **10**, 502 (1985).
[21]A. H. Kung, Opt. Lett. **8**, 24 (1983).
[22]C. T. Rettner, E. E. Marinero, R. N. Zare, and A. H. Kung, J. Phys. Chem. **88**, 4459 (1984).
[23]R. H. Page, R. J. Larkin, A. H. Kung, Y. R. Shen, and Y. T. Lee, Rev. Sci. Instrum. **58**, 1616 (1987).
[24]E. Cromwell, T. Trickl, Y. T. Lee, and A. H. Kung, Rev. Sci. Instrum. **60**, 2888 (1989).
[25]U. Hollenstein, H. Palm, and F. Merkt, Rev. Sci. Instrum. **71**, 4023 (2000).
[26]V. E. Peet and R. V. Tsubin, Opt. Commun. **214**, 381 (2002).
[27]S. Hannemann, U. Hollenstein, E.-J. van Duijn, and W. Ubachs, Opt. Lett. **30**, 1494 (2005).
[28]J. Darginavičius, G. Tamošauskas, G. Valiulis, and A. Dubietis, Opt. Commun. **282**(4), 2995 (2009).
[29]J. Darginavičius, G. Tamosauskas, A. Piskarkas, and A. Dubietis, Opt. Express **18**, 16096 (2010).
[30]J. L. Silva, H. Crespo, and R. Weigand, Appl. Opt. **50**, 1968 (2011).
[31]R. Weigand and H. M. Crespo, Appl. Phys. B **111**, 559 (2013).
[32]R. Hector and K. H. Meiwes-Broer, Opt. Commun. **123**, 155 (1996).
[33]S. Chénais, S. Forget, L. Philippet, and M.-C. Castex, Appl. Phys. B **89**, 223 (2007).
[34]M. L. Huber, A. Laesecke, and D. G. Friend, NISTIT 6643, Boulder, CO, 2006.
[35]L. Museur, W. Q. Zheng, A. V. Kanaev, and M. C. Castex, IEEE J. Sel. Top. Quantum Electron. **1**, 900 (1995).
[36]L. Museur, C. Olivero, D. Riedel, and M. C. Castex, Appl. Phys. B **70**, 499 (2000).
[37]J. Wang, B. Yang, T. A. Cool, N. Hansen, and T. Kasper, Int. J. Mass Spectrom. **269**, 210 (2008).
[38]J. C. Person and P. P. Nicole, J. Chem. Phys. **53**, 1767 (1970).
[39]N. Bras, J. C. Jeannet, and D. Perrin, J. Phys. B **26**, 2289 (1993).
[40]G. C. Bjorklund, IEEE J. Quantum Electron. **11**, 287 (1975).
[41]A. V. Smith and W. J. Alford, Phys. Rev. A **33**, 3172 (1986).
[42]A. Kramida, Y. Ralchenko, J. Reader, and NIST ASD Team, NIST Atomic Spectra Database (ver 5.0), National Institute of Standards and Technology, Gaithersburg, MD, 2012, available at online: http://physics.nist.gov/asd (July 5 2013).
[43]A. Bogaerts, Z. Y. Chen, R. Gijbels, and A. Vertes, Spectrochim. Acta, Part B **58**, 1867 (2003).
[44]S. A. Meyer and G. W. Faris, Opt. Lett. **23**, 204 (1998).
[45]E. E. Marinero, C. T. Rettner, R. N. Zare, and A. H. Kung, Chem. Phys. Lett. **95**, 486 (1983).
[46]V. V. Slabko, A. K Popov, and V. F. Lukinykh, Appl. Phys. **15**, 239 (1977).
[47]W. R. Hunter, "Reflectance spectra of single Materials," in *Vacuum Ultraviolet Spectroscopy*, edited by J. A. Samson and D. L. Ederer (Academic Press, San Diego, 2000), pp. 205–225.
[48]S. G. Lias, "Ionization energy Evaluation," in *NIST Chemistry, WebBook, NIST Standard Reference Database Number 69*, edited by P. J. Linstom and W. G. Mallard (Nation Institute of Standards Technology, Gaithersburg, MD, 2015), http://webbook.nist.gov (retrieved September 30, 2015).